

Electrochemical Synthesis of the Composites Based on Multi-Wall Carbon Nanotubes and Polypyrrole Doped with Phosphomolybdic Acid Heteropolyanions and Their Vibrational Properties

M. Baibarac^{1,*}, C. Serbschi², M. Stroe¹

¹ National Institute of Materials Physics, Lab. Optical Processes in Nanostructured Materials, P.O. Box MG-7, Bucharest, R077125, Romania

² Bioelectronic SRL, Cercelus street, no.54, Ploiesti, Romania

*E-mail: barac@infim.ro

Received: 17 June 2018 / Accepted: 20 August 2018 / Published: 1 October 2018

Using cyclic voltammetry, Raman scattering and infrared (IR) spectroscopy, new findings concerning the electrochemical synthesis of composites based on multi-wall carbon nanotubes (MWNTs) and polypyrrole (PPY) doped with $\text{H}_3\text{PMo}_{12}\text{O}_{40}$ heteropolyanions are described in this report. To better understand the electrochemical mechanism behind the synthesis of these composites, the influence of the concentrations of pyrrole and the electrolytes of $\text{H}_3\text{PMo}_{12}\text{O}_{40}$ and H_2SO_4 on the cyclic voltammogram profile is studied. The formation of PPY doped with $\text{H}_3\text{PMo}_{12}\text{O}_{40}$ heteropolyanions onto the MWNT surface is demonstrated by complementary studies of Raman scattering and IR spectroscopy.

Keywords: carbon nanotubes, polypyrrole, cyclic voltammetry

1. INTRODUCTION

The interest in conjugated polymers doped with heteropolyanions of Keggin acids dates back to 1995 when the first strategies for the chemical polymerization of pyrrole in the presence of phosphomolybdic acid ($\text{H}_3\text{PMo}_{12}\text{O}_{40}$) were established. [1] This method was later used for the chemical synthesis of other conjugated polymers, such as polyaniline [2] and poly(3,4-ethylenedioxithiophene) [3]. The development of new synthetic methods, such as the vapor transport of monomers over carbon paper [4] and the electrochemical polymerization of monomers [5] in the presence of oxidative solutions of heteropolyacids, have enabled the use of polypyrrole doped with heteropolyanions of $\text{H}_3\text{PMo}_{12}\text{O}_{40}$ (PPY-PMo12) in a wide range of applications, including as active

electrode materials in the supercapacitor field [4, 5], in the amperometric detection of catecholamines [6], as a nitric oxide sensor [7] and as an electrochemical sensor for the folic acid detection [8]. Beginning in 2005, special attention was given to the composite materials of conjugated polymers doped with heteropolyanions of Keggin acids and carbon nanoparticles, such as carbon nanotubes and graphene [9, 10]. The achievement of new composites of the type PPY-PMo12/carbon nanoparticles was demonstrated by applications in the fields of the sensitive determination of folic acid [10], photocatalysis [11] and the electrocatalytic reduction of bromate [12]. Despite this progress and the best efforts of the authors, there is no systematic study on the electrochemical polymerization process of composites based on PPY-PMo12 and carbon nanotubes. Therefore, in this paper, attention will be focused on the influence of the conditions imposed on the electrochemical synthesis of composites based on PPY-PMo12 and multi-walled carbon nanotubes (MWNTs) and the cyclic voltammogram features that describe this process, as well as the vibrational properties of these materials.

2. EXPERIMENTAL

The chemical compounds required in this study, i.e., pyrrole, H_2SO_4 and $\text{H}_3\text{PMo}_{12}\text{O}_{40}\cdot x\text{H}_2\text{O}$, were purchased from Sigma-Aldrich.

The electropolymerization of pyrrole in the presence of $\text{H}_3\text{PMo}_{12}\text{O}_{40}\cdot x\text{H}_2\text{O}$ was performed by cyclic voltammetry using a gold plate or a gold support covered with a MWNT film (with a thickness of 100 nm) as the working electrode. The electrochemical cell contained three electrodes, i.e., the working electrode, the counter electrode consisting of a Pt wire and a saturated calomel electrode (SCE) as the reference electrode, and was connected to a potentiostat/galvanostat (Voltalab 80 from Radiometer Analytical) to record the cyclic voltammograms reported in this work. All voltammograms were recorded in the potential range (-0.2; +0.8) V vs. SCE with a sweep rate of 100 mV s^{-1} .

The Raman spectra of MWNTs, PPY-PMo12 and the PPY-PMo12/MWNTs composites were recorded using a Raman spectrophotometer (T64000 model from Horiba Jobin Yvon), which utilized an Ar laser. The Raman spectra of pyrrole and the MWNTs functionalized with pyrrole were recorded using an FT Raman spectrophotometer (RFS100S model from Bruker).

The IR spectra of PPY-PMo12 and the PPY-PMo12/MWNTs composites were recorded using a FTIR spectrophotometer (Vertex 70 model from Bruker).

3. RESULTS AND DISCUSSION

Figure 1 shows the first 25 cyclic voltammograms recorded with the blank Au electrode and the Au plate covered with a MWNT film when the working electrode was immersed in a solution of 0.5 M H_2SO_4 and $5 \times 10^{-3} \text{ M H}_3\text{PMo}_{12}\text{O}_{40}$ with a pyrrole concentration of $1.5 \times 10^{-2} \text{ M}$ (a), $3 \times 10^{-2} \text{ M}$ (b) and $6 \times 10^{-2} \text{ M}$ (c). In all six cases, the cyclic voltammograms show in the potential ranges (-0.2; 0), (0, +0.25) and (+0.25; +0.5) V three oxidation maxima labeled A_1 , B_1 and C_1 that are accompanied by three reduction maxima designated A_2 , B_2 and C_2 , respectively. In Table 1, the variation in the

oxidation and reduction potentials in the case of the second and 25th cyclic voltammograms is given for the six cases shown in Figure 1.

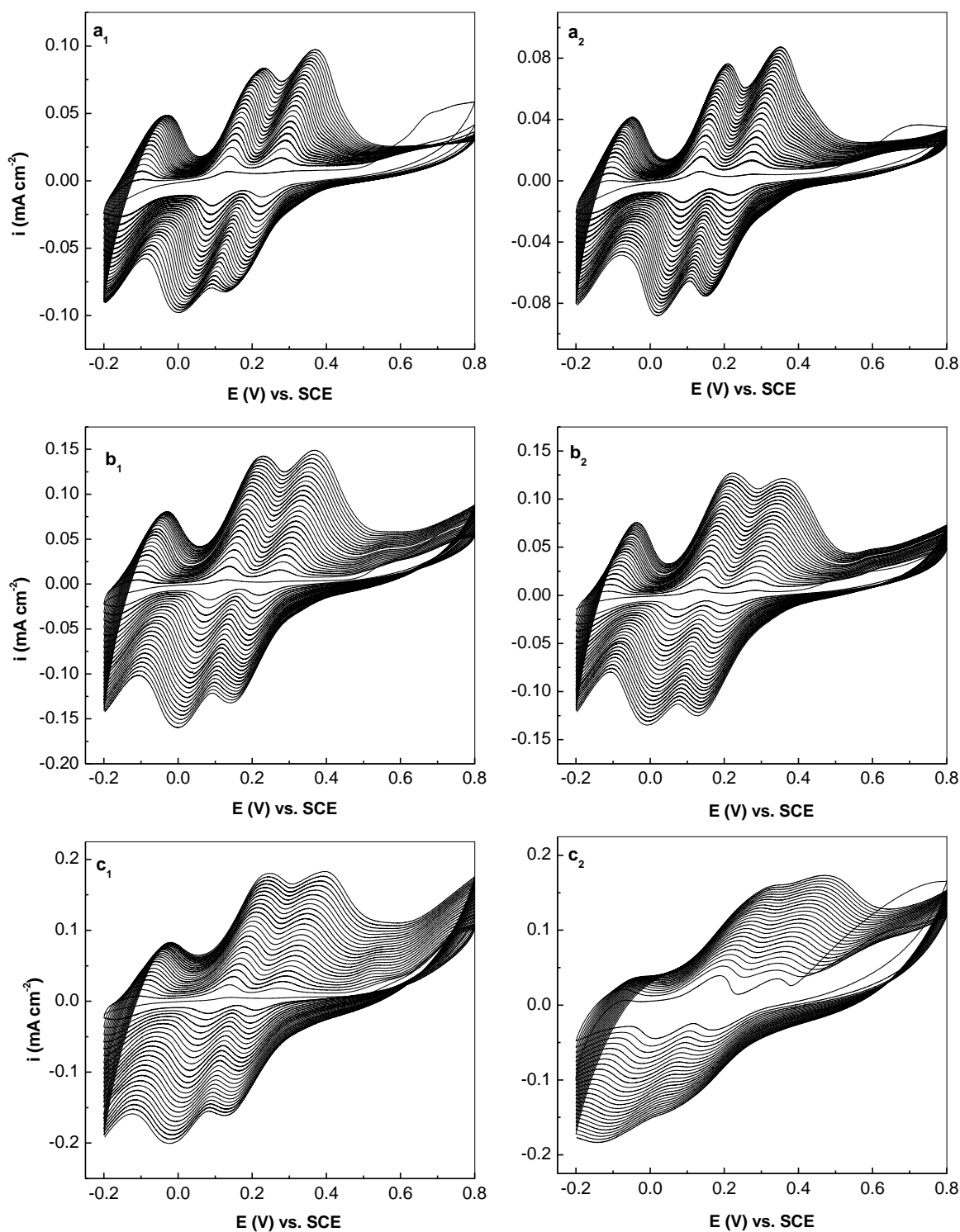


Figure 1 The first 25 cyclic voltammograms that describe the electropolymerization of pyrrole onto the blank Au electrode (1) and the Au plate covered with a MWNT film (2) when each working electrode was immersed in a solution of 0.5 M H_2SO_4 , 5×10^{-3} M $\text{H}_3\text{PMO}_{12}\text{O}_{40}$ and pyrrole with a concentration of: 1.5×10^{-2} M (a), 3×10^{-2} M (b) and 6×10^{-2} M (c).

Table 1. The change in the potentials of the anodic and cathodic peaks (E_{pa} and E_{pc}) with increasing cyclic voltammogram number when each working electrode was immersed in a solution of 0.5 M H_2SO_4 , 5×10^{-3} M $H_3PMo_{12}O_{40}$ and different pyrrole concentrations. $\Delta E = E_{pa} - E_{pc}$ = the separation between the anodic and cathodic peaks potential

Working electrode	Pyrrole concentration (M)	Cycle number	E_{pa} (mV) of A ₁ , B ₁ and C ₁ peak	E_{pc} (mV) of A ₂ , B ₂ and C ₂ peak	ΔE (mV)
Au	1.5×10^{-2}	2	-103, +138, +277	-154, +91, +227	51, 47, 50
Au	1.5×10^{-2}	25	-31, +230, +370	-195, -3, +128	164, 233, 242
Au	3×10^{-2}	2	-113, +137, +275	-144, +86, +222	31, 51, 53
Au	3×10^{-2}	25	-30, +235, +380	-195, -2, +143	165, 237, 237
Au	6×10^{-2}	2	-105, +135, +274	-148, +82, +211	43, 53, 63
Au	6×10^{-2}	25	-22, +242, +401	-195, -22, +128	173, 264, 273
MWNT/Au	1.5×10^{-2}	2	-115, +137, +274	-153, +86, +222	38, 51, 52
MWNT/Au	1.5×10^{-2}	25	-47, +208, +351	-194, +16, +152	147, 192, 199
MWNT/Au	3×10^{-2}	2	-124, +141, +281	-162, +76, +209	38, 65, 72
MWNT/Au	3×10^{-2}	25	-36, +222, +362	-194, -9, +129	158, 231, 233
MWNT/Au	6×10^{-2}	2	-78, +188, +340	+13, +170	175, 170
MWNT/Au	6×10^{-2}	25	-40, +323, +477	-139, +51	462, 426

According to Figure 1 and Table 1, with increasing cyclic voltammogram number from 2 to 25, one observes an increase in the oxidation and reduction current densities, as well as the separation potential of the anodic and cathodic peaks. This fact indicates that the deposition of PPY took place on the blank Au electrode and the Au plate covered with a MWNT film. In the case of the blank Au support, with increasing pyrrole concentration in the solution of 0.5 M H_2SO_4 and 5×10^{-3} M $H_3PMo_{12}O_{40}$, for the 25th cyclic voltammogram, one observes an increasing of the potential of separation of the anodic and cathodic peaks, as well as the current densities of the oxidation and reduction maxima. An intriguing experimental result is shown in Figure 1c₂. In the case of the Au electrode covered with a MWNT film immersed in a solution of 0.5 M H_2SO_4 , 5×10^{-3} M $H_3PMo_{12}O_{40}$ and 6×10^{-2} M pyrrole, during the cathodic sweep, only two reduction peaks situated at -139 and +51 mV are observed. This experimental result, as well as the increased values of the potential of separation of the anodic and cathodic peaks at the end of the 25th cyclic voltammogram in the six cases (Table 1), indicates that the electrochemical processes shown in Figure 1 have an irreversible character.

Figures 2 and 3 show the variations in the cyclic voltammograms that describe the electropolymerization of pyrrole induced by the change in the concentration of $H_3PMo_{12}O_{40}$ and H_2SO_4 , respectively.

Tables 2 and 3 give the changes in the potentials of the anodic and cathodic peaks (E_{pa} and E_{pc}) with increasing concentrations of $H_3PMo_{12}O_{40}$ and H_2SO_4 in the synthesis solutions of PPY and its composites with MWNTs. According to Table 2, a decrease in the $H_3PMo_{12}O_{40}$ concentration in the solution of 0.5 M H_2SO_4 and 3×10^{-2} M pyrrole induces a decrease in both the potential of separation of the anodic and cathodic peaks and the current densities of the oxidation and reduction maxima for

both types of working electrodes. This result is in good agreement with the studies reported by Y. Li and J. Yang. [13]

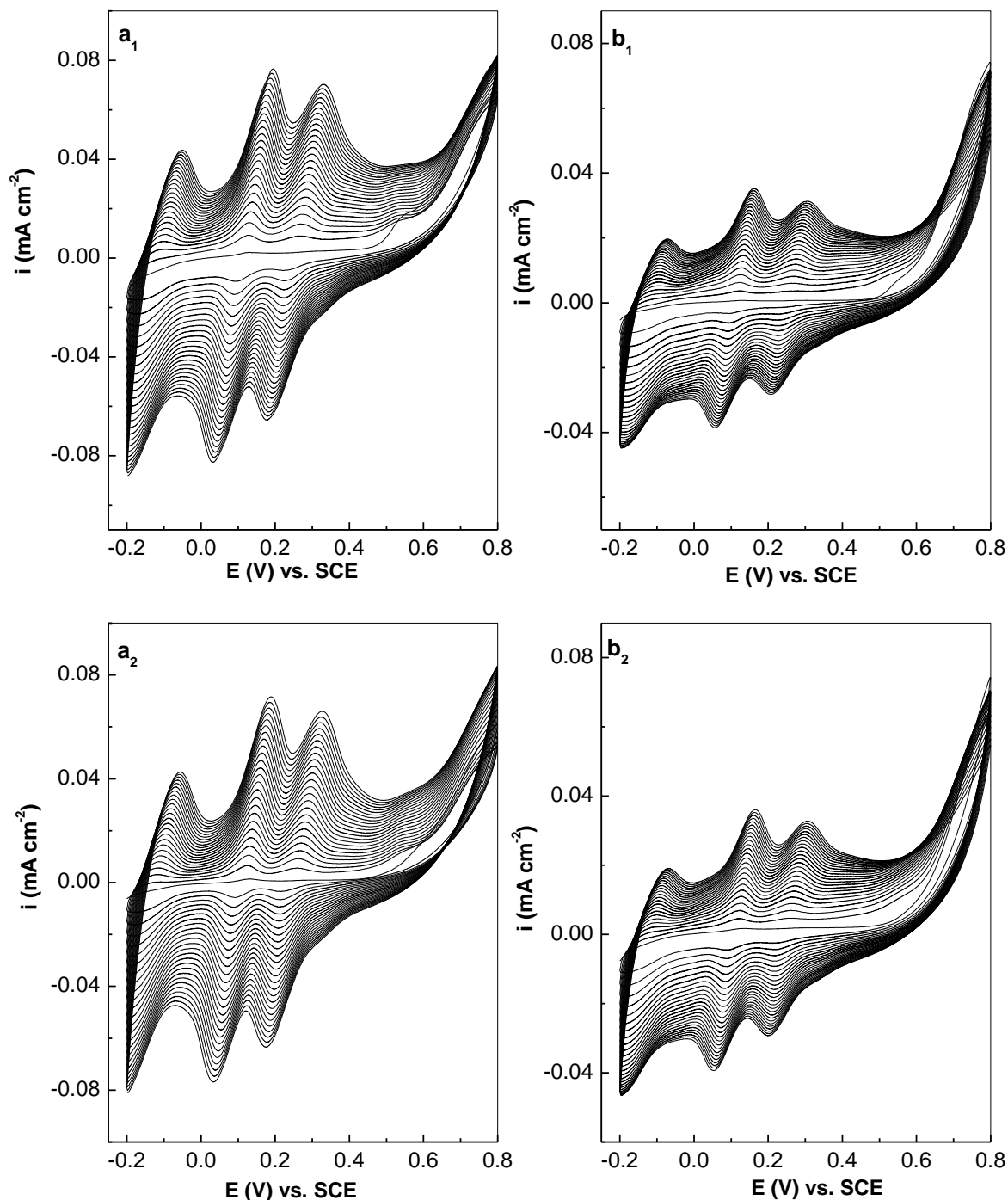


Figure 2 Cyclic voltammograms that describe the electropolymerization of pyrrole onto the blank Au electrode (1) and the Au plate covered with a MWNT film (2), when each working electrode was immersed in a solution of 0.5 M H_2SO_4 , 3×10^{-2} M pyrrole and $\text{H}_3\text{PMo}_{12}\text{O}_{40}$ with a concentration equal to 2.5×10^{-3} M (a) or (b) and 1.25×10^{-3} M.

No significant variation in the potential of separation of the anodic and cathodic peaks, as well as the current densities of the oxidation and reduction maxima for the same cycle number, and a

constant $\text{H}_3\text{PMo}_{12}\text{O}_{40}$ concentration in the solution of 0.05 M H_2SO_4 and 3×10^{-2} M pyrrole is observed in Figure 2 and Table 2.

Table 2. The change in the potentials of the anodic and cathodic peaks (E_{pa} and E_{pc}) with increasing $\text{H}_3\text{PMo}_{12}\text{O}_{40}$ concentration in the solution of 0.05 M H_2SO_4 and 3×10^{-2} M pyrrole

Working electrode	$\text{H}_3\text{PMo}_{12}\text{O}_{40}$ concentration	Cycle number	E_{pa} (mV) of A ₁ , B ₁ and C ₁ peak	E_{pc} (mV) of A ₂ , B ₂ and C ₂ peak	ΔE (mV)
Au	2.5×10^{-3} M	25	-51, +194, +331	-194, +31, +178	143, 163, 153
Au	1.25×10^{-3} M	25	-70, +161, +305	-197, +53, +207	127, 108, 98
MWNT/Au	2.5×10^{-3} M	25	-54, +190, +326	-197, +33, +178	143, 157, 148
MWNT/Au	1.25×10^{-3} M	25	-71, +166, +307	-197, +53, +199	126, 113, 108

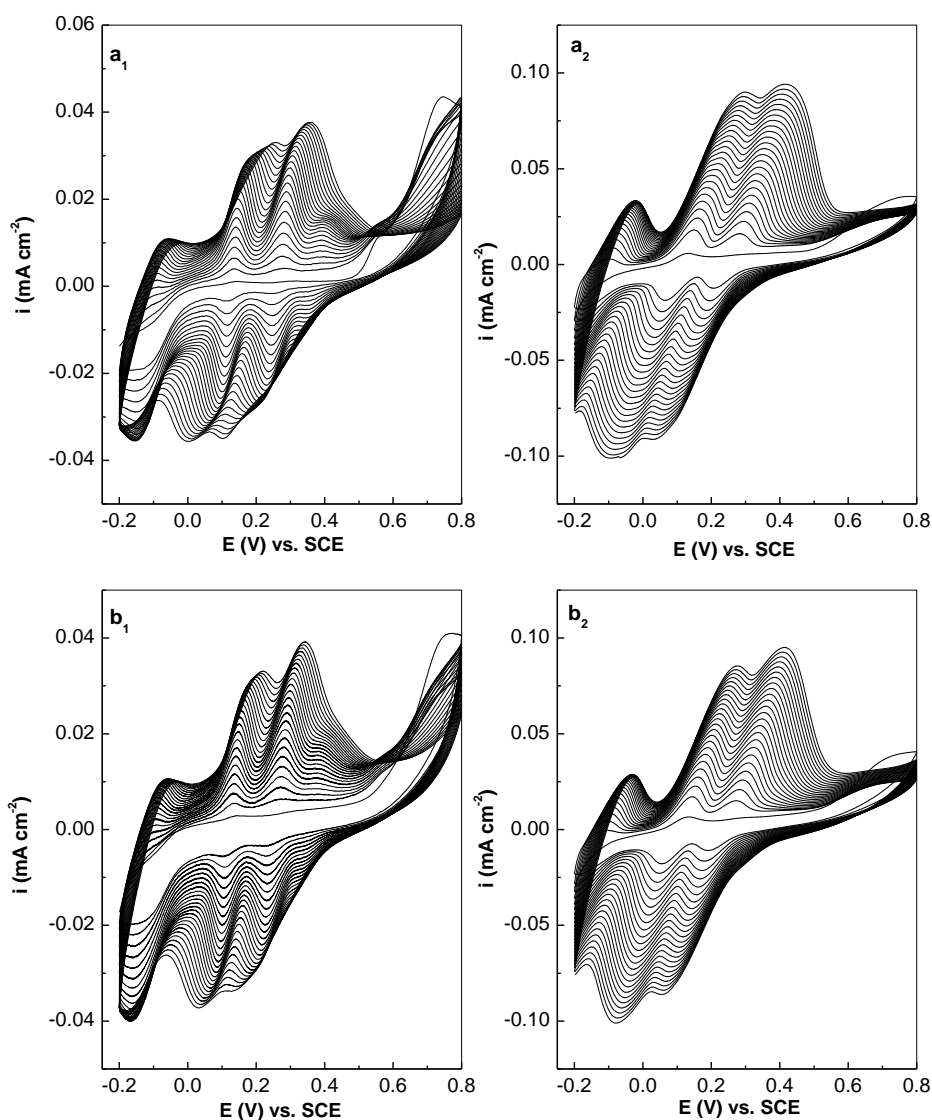


Figure 3 Cyclic voltammograms that describe the electropolymerization of pyrrole onto the blank Au electrode (1) and the Au plate covered with a MWNT film (2) when each working electrode was immersed in a solution of 3×10^{-2} M pyrrole, 5×10^{-3} M $\text{H}_3\text{PMo}_{12}\text{O}_{40}$ and 1 M H_2SO_4 (a) or 0.25 M H_2SO_4 (b).

A different result is observed with the variation of the H_2SO_4 concentration in the solution of 5×10^{-3} M $\text{H}_3\text{PMo}_{12}\text{O}_{40}$ and 3×10^{-2} M pyrrole. Figure 3 and Table 3 are relevant in this sense.

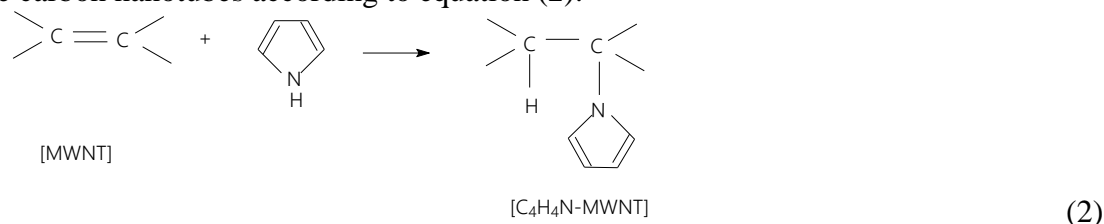
Table 3. The change in the potentials of the anodic and cathodic peak (E_{pa} and E_{pc}) with increasing H_2SO_4 concentration in the solution of 5×10^{-3} M $\text{H}_3\text{PMo}_{12}\text{O}_{40}$ and 3×10^{-2} M pyrrole

Working electrode	H_2SO_4 concentration	Cycle number	E_{pa} (mV) of A_1 , B_1 and C_1 peak	E_{pc} (mV) of A_2 , B_2 and C_2 peak	ΔE (mV)
Au	1 M	25	-34, +249, +361	-151, -1, +105	117, 250, 256
Au	0.25 M	25	-24, +297, +416	-44, +220, +341	20, 77, 75
MWNT/Au	1 M	25	-44, +220, +341	-165, +27, +142	121, 193, 199
MWNT/Au	0.25 M	25	-30, +275, +415	-, -84, +57	-, 359, 358

As observed in Table 3, the decreasing H_2SO_4 concentration in the solution of 5×10^{-3} M $\text{H}_3\text{PMo}_{12}\text{O}_{40}$ and 3×10^{-2} M pyrrole leads to a decrease in the value of the potential of separation of the anodic and cathodic peaks, when a gold plate is used as the working electrode. A different behavior is observed in the case of the Au support covered with a MWNT film. According to Figures 3a₂ and 3b₂, the cyclic voltammograms are characterized by three oxidation peaks and two reduction peaks, the values of the potential of separation of the last two anodic/cathodic peaks situated at +220/+27, +341/+142, +275/-84 and +415/+57 mV (Table 3) increase when the H_2SO_4 concentration in the solution of 5×10^{-3} M $\text{H}_3\text{PMo}_{12}\text{O}_{40}$ and 3×10^{-2} M pyrrole increases. Summarizing the above results, we conclude that the presence of MWNTs on the Au electrode surface induces changes in the reaction mechanism of the synthesis of PPY in the presence of $\text{H}_3\text{PMo}_{12}\text{O}_{40}$ and H_2SO_4 . In our opinion, a reaction similar to that proposed in Ref. [14] can occur in the case of the Au electrode, as follows:



In the presence of MWNTs, the electrochemical reactions are preceded by a chemical reaction between pyrrole and the carbon nanotubes according to equation (2):



Furthermore, the electropolymerization reaction of MWNTs covalently functionalized with pyrrole molecules takes place as follows:



Information about the vibrational properties of the composite material is further shown by Raman scattering and IR spectroscopy. Figure 4a shows the Raman spectrum of PPY-PMo12. In the spectral range $800\text{-}1750 \text{ cm}^{-1}$, the main Raman lines of the PPY doped with the $\text{H}_3\text{PMo}_{12}\text{O}_{40}$ heteropolyanions are peaked at 942, 996, 1059, 1085, 1374 and 1603 cm^{-1} , and they are assigned to the following vibrational modes: ring deformation associated with a dication, ring deformation associated

with a radical cation, in-plane symmetric bending of the polaron structure, C_{β} -H in-plane symmetric bending, antisymmetric $N-C_{\alpha}$ stretching and $C_{\alpha}=C_{\beta}$ stretching + $C_{\alpha}=C_{\beta}$ intra-ring + $C_{\alpha}-C_{\alpha'}$ inter-ring stretching. [15-20]

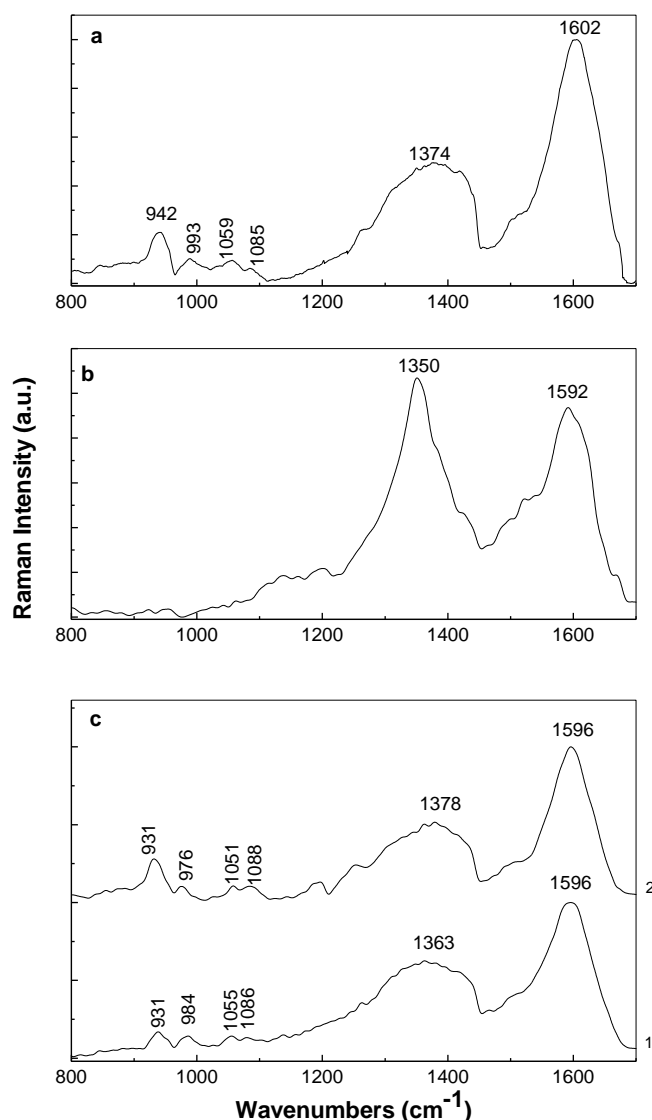


Figure 4 Raman spectra of the PPY doped with the $H_3PMO_{12}O_{40}$ heteropolyanions (a), MWNTs (b) and the composite based on the PPY doped with the $H_3PMO_{12}O_{40}$ heteropolyanions and MWNTs obtained by performing 10 (curve 1 in Figure c) and 50 cyclic voltammograms (curve 2 in Figure c) when each working electrode was immersed in a solution of 3×10^{-2} M pyrrole, 5×10^{-3} M $H_3PMO_{12}O_{40}$ and 0.5 M H_2SO_4 . The excitation wavelength was 514 nm.

Figure 4b shows the Raman spectrum of the MWNT film deposited onto the Au electrode, which is characterized by two Raman bands at 1350 and 1590 cm⁻¹ and assigned to the defects or disordered state in the graphitic lattice and the tangential mode, respectively. [21] Curves 1 and 2 in Figure 4c show the Raman spectra of the composite based on PPY doped with the $H_3PMO_{12}O_{40}$ heteropolyanions and MWNTs, synthesized during the recording of 10 and 50 cyclic voltammograms. The main differences in the Raman spectra of the composite materials regard: i) the downshift of the Raman lines assigned to the vibrational mode of ring deformation associated with the dication and

radical cation structures of PPY, from 942 and 996 cm^{-1} (Figure 4a) to 931 and 984 - 976 cm^{-1} (Figure 4c); ii) the change in the ratio of the Raman lines at 931 and 984 - 976 cm^{-1} from 1:1 (curve 1 in Figure 4c) to 2:1 (curve 2 in Figure 4c); and iii) the downshift of the Raman lines attributed to the vibrational mode in-plane symmetric bending of the polaron structure and $\text{C}_\alpha=\text{C}_\beta$ stretching + $\text{C}_\alpha=\text{C}_\beta$ intra-ring + $\text{C}_\alpha-\text{C}_\alpha'$ inter-ring stretching, from 1059 and 1603 cm^{-1} (Figure 4a) to 1055 cm^{-1} (curve 1 in Figure 4c) or 1051 cm^{-1} (curve 2 in Figure 4c) and 1596 cm^{-1} (Figure 4c), respectively. These changes clearly reveal that a chemical reaction between PPY or its precursor, namely, pyrrole molecules, and MWNTs took place during the electrosynthesis of the composite material.

The information concerning the presence of the $\text{H}_3\text{PMo}_{12}\text{O}_{40}$ heteropolyanions in the composite mass is shown in Figure 5.

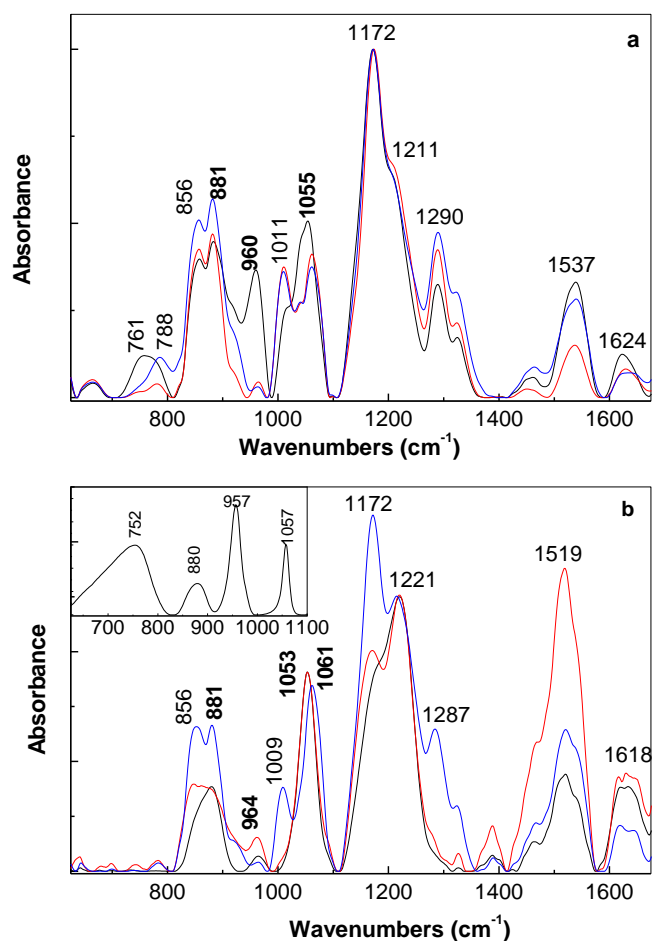


Figure 5 IR absorption spectra of the PPY doped with the $\text{H}_3\text{PMo}_{12}\text{O}_{40}$ heteropolyanions in the absence (a) and the presence of MWNTs (b) when the composites were synthesized using a solution consisting of 3×10^{-2} M pyrrole, 0.5 M H_2SO_4 and $\text{H}_3\text{PMo}_{12}\text{O}_{40}$ with a concentration of: 5×10^{-3} M (black curve), 2.5×10^{-3} M (red curve) and 1.25×10^{-3} M (blue curve).

As shown in the insert of Figure 5b, the IR bands of $\text{H}_3\text{PMo}_{12}\text{O}_{40}$ are at 752, 880, 957 and 1057 cm^{-1} , with these being assigned to the vibrational modes of the edge Mo-O-Mo, vertex Mo-O-Mo, terminal Mo=O and P-O, respectively. [5] Figure 5a shows the IR spectra of the PPY doped with the $\text{H}_3\text{PMo}_{12}\text{O}_{40}$ heteropolyanions when the concentration of the heteropolyacid in the synthesis solution

varied from 2.5×10^{-3} M to 1.25×10^{-3} M. The main IR bands of the PPY are at 856, 1011-1172, 1211, 1290, 1537 and 1624 cm^{-1} , and they are assigned to the following vibrational modes: C-H out-of-plane bending, polaron and bipolaron structure bending, C-H in-plane bending, N-C in-plane bending, C=C [22] and PPY in the oxidized state, respectively [23]. Depending on the $\text{H}_3\text{PMo}_{12}\text{O}_{40}$ concentration, the following changes are observed in Figure 5a with decreasing heteropolyacid concentration: i) an up-shift of the IR band assigned to the vibrational mode of the edge Mo-O-Mo from 761 to 788 cm^{-1} , accompanied of a decrease in the absorbance of the vibrational mode of the terminal Mo=O; and ii) a gradual decrease in the absorbance of the IR bands assigned to the vibrational modes of C=C and the oxidized state of PPY. These changes must be understood as a consequence of the compensation of the positive charges that are on the PPY macromolecular backbone with $\text{H}_3\text{PMo}_{12}\text{O}_{40}$ heteropolyanions. Regardless of the $\text{H}_3\text{PMo}_{12}\text{O}_{40}$ concentration in the synthesis solution, in the presence of MWNTs, the disappearance of the vibrational mode of the edge Mo-O-Mo is observed in Figure 5b. This fact can be understood only as a result of a MWNT-induced shielding process of PPY doped with the $\text{H}_3\text{PMo}_{12}\text{O}_{40}$ heteropolyanions. Other changes observed in Figure 5 consist of: i) the simultaneous downshift of the IR band assigned to the vibrational mode of C=C in PPY, from 1537 cm^{-1} (Figure 5a) to 1519 cm^{-1} (Figure 5b), and gradual increase in its absorbance with decreasing $\text{H}_3\text{PMo}_{12}\text{O}_{40}$ concentration in the synthesis solution; and ii) an increase in the absorbance of the IR bands assigned to the vibrational modes of polaron and bipolaron structures' bending and C-H out-of-plane bending when the heteropolyacid concentration was 1.25×10^{-3} M. In our opinion, these variations can be explained only if it is accepted that a covalent functionalization process of MWNTs with the pyrrole molecules takes place.

To support this statement, Figure 6 shows Raman spectra of pyrrole (PY), MWNTs and mixtures of the two constituents having PY:MWNT weight ratios of 97:1 and 97:10. The mixtures of the two compounds were ultrasonicated for 30 min. In the spectral range of 1100 to 1700 cm^{-1} , the main Raman lines of PY are situated at 1145 , 1382 and 1469 cm^{-1} , with these being assigned to the following vibrational modes of bonds: CH stretching, CH in-plane deformation and CH out-of-plane deformation, respectively. [24, 25] The addition of MWNTs to the PY mass involves a chemical interaction that induces the following changes in the Raman spectra of the two constituents: i) The appearance of the two Raman lines of MWNTs, at 1286 and 1600 - 1603 cm^{-1} (red and blue curves in Figure 6), belonging to the disordered state or the defect-induced graphene lattice of carbon nanotubes (D band) and the tangential mode (TM band), respectively [21]; in this context, with increasing MWNT weight in the PY mass, an increase in the relative intensity of these Raman lines of carbon nanotubes is also observed. ii) A downshift of the Raman line of PY, situated in the 1100 - 1170 cm^{-1} spectral range, from 1145 to 1141 cm^{-1} simultaneously with an increase of its half-width as the MWNT weight in the PY mass increases. iii) A gradual decrease in the relative intensity of the Raman line of PY peaked in the 1300 - 1400 cm^{-1} spectral range. iv) The value of the ratio between the relative intensities of the D and TM bands (I_D/I_{TM}) varies from 0.82 to 0.93 and 1.1 for the case of MWNTs and the mixtures having PY:MWNT weight ratios equal to 97:1 and 97:10, respectively.

The downshift of the Raman lines at 1145 - 1141 and 1603 - 1600 cm^{-1} , assigned to the CH stretching vibrational mode and tangential mode of carbon nanotubes, and the decrease in the relative intensity of the Raman line at 1382 cm^{-1} , attributed to the CH bond in-plane deformation vibrational

mode, as well as the variation of the I_D/I_{TM} ratio are evidence that indicate a covalent functionalization of carbon nanotubes with pyrrole molecules occurs.

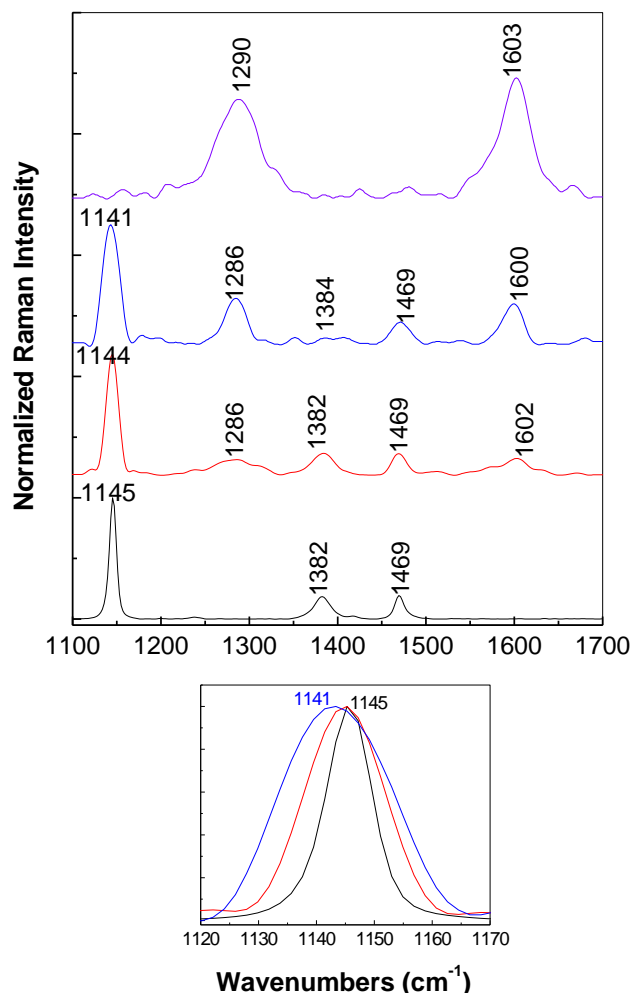


Figure 6 Raman spectra of PY (black curve), MWNTs (violet curve) and mixtures of Py:MWNTs having weight ratios equal to 97:1 (red curve) and 97:10 (blue curve). All spectra were recorded with an excitation wavelength of 1064 nm.

Taking into account all the data, the above results of Raman scattering and IR absorption spectroscopy demonstrate that the electrochemical polymerization reaction of pyrrole covalently functionalized MWNTs in the presence of $H_3PMO_{12}O_{40}$ leads to the formation of MWNTs covalently functionalized with PPY doped with the heteropolyacid anions.

4. CONCLUSIONS

In this report, new data concerning the electrochemical synthesis of composites based on PPY doped with the $H_3PMO_{12}O_{40}$ heteropolyanions and MWNTs are presented. The highlights of this work consist of the following:

i) The demonstration that the electropolymerization of pyrrole in the presence of $\text{H}_3\text{PMo}_{12}\text{O}_{40}$ and H_2SO_4 corresponds to an irreversible process, regardless of the working electrode being a blank Au support or a gold plate covered with a MWNT film. The increase of the pyrrole concentration in the synthesis solution leads to the formation of a large amount of polymer on the working electrode surface, as highlighted by the increases of the anodic and cathodic current densities. The increase in the electrolyte concentration of the PPy synthesis solution leads to the compensation of the positive charges of the PPy macromolecular backbone with $\text{H}_3\text{PMo}_{12}\text{O}_{40}$ heteropolyanions.

ii) The electropolymerization reaction of the pyrrole in the presence of $\text{H}_3\text{PMo}_{12}\text{O}_{40}$, H_2SO_4 and MWNTs is preceded by a chemical reaction between pyrrole and MWNTs molecules, which leads to a covalent functionalization process of MWNTs with pyrrole molecules. Using Raman scattering and IR absorption spectroscopy, we demonstrate that the composite obtained by the electrochemical polymerization of pyrrole in the presence of $\text{H}_3\text{PMo}_{12}\text{O}_{40}$, H_2SO_4 and MWNTs corresponds to MWNTs covalently functionalized with PPy doped with the $\text{H}_3\text{PMo}_{12}\text{O}_{40}$ heteropolyanions.

ACKNOWLEDGMENTS

This work was funded by the project co-funded by the European Regional Development Fund under the Competitiveness Operational Program 2014-2020, titled "Physico-chemical analysis, nanostructured materials and devices for applications in the pharmaceutical field and medical in Romania", the financing contract no. 58/05.09.2016 signed of National Institute of Materials Physics with National Authority for Scientific Research and Innovation as an Intermediate Body on behalf of the Ministry of European Funds as Managing Authority for Operational Program Competitiveness (POC), the subcontract of the D type, no. 2626/04.12.2017, signed by the National Institute of Materials Physics with Bioelectronic SRL.

References

1. M.S. Freund, C. Karp and N.S. Lewis, *Inorg. Chim. Acta*, 240 (1995) 447.
2. P. Gomez-Romero, N. Casan-Pastor and M. Lira-Cantu, *Solid State Ionics*, 101-103 (1997) 875.
3. M.B. McDonald and M.S. Freund, *ACS Appl. Mater. Inter.*, 3 (2011) 1009.
4. A.M. Wjote and R.C.T. Slade, *Electrochim. Acta*, 48 (2003) 2583.
5. A.K. Cuentas-Gallegos, M. Lira-Cantu, N. Casan-Pastor and P. Gomez-Romero, *Adv. Funct. Mater.*, 15 (2008) 1125.
6. A. Liu and E. Wang, *Anal. Chim. Acta*, 296 (1994) 171.
7. Y. Zhang, Y. A. Si, W.N. Do, T. Yang, *Advanced Materials Research*, 634-638 (2013) 3862.
8. H.X. Guo, Y.Q. Li, L.F. Fan, X.Q. Wu and M.D. Guo, *Electrochim. Acta*, 51 (2006) 6230.
9. J. Chen, S. Liu, W. Feng, G. Zhang and F. Yang, *Phys. Chem. Chem. Phys.*, 15 (2013) 5664.
10. Z. Wang, Q. Han, J. Xia, L. Xia, S. Bi, G. Shi, F. Zhang, Y. Xia, Y. Li and L. Xia, *J. Electroanal. Chem.*, 726 (2014) 107.
11. Q.Y. Tang, X.X. Luo and R.M. Wen, *Anal. Lett.*, 38 (2005) 1445.
12. M. Skunik, P.J. Kulesza, *Anal. Chim. Acta*, 630 (2009) 153.
13. Y. Li, J. Yang, *J. Appl. Polym. Sci.*, 65 (1997) 2739.
14. T. Ohtsuka, T. Wakabayashi, H. Einaga, *J. Electroanal. Chem.*, 377 (1994) 107.
15. R. Koarix, D. Rakovic, S.A. Stepanyan, I.E. Davidova and L.A. Gribov, *J. Chem. Phys.*, 102 (1995) 3104.
16. Y.C. Liu and B.J. Hwang, *Synth. Met.*, 113 (2000) 203.

17. E. Faulques, W. Wallnofer and H. Kuzmany, *J. Chem. Phys.*, 90 (1989) 7585.
18. X. Zhu, Y. Shen, Z. Peng, L. Zhang, L. Bi, Y. Wang and S. Dong, *J. Electroanal. Chem.*, 566 (2004) 63.
19. K. Crowley and J. Cassidy, *J. Electroanal. Chem.*, 547 (2003) 75.
20. S. Demoustier-Champagne and P.Y. Stavaus, *Chem. Mater.*, 11 (1999) 829
21. M.S. Dresselhaus, G. Dresselhaus and P.C. Eklund, *Science of fullerenes and carbon nanotubes*, Academic Oress, New York (1996).
22. M. L. Daroux, E. B. Yeager, M. Kalaji, N. H. Cuong and A. Bewick, *Macromol. Chem. Macromol. Symp.*, 8 (1987) 127.
23. J. Przluski, M. Zagorska, A. Pron, Z. Kucharski and J. Suwalski, *J. Phys. Chem. Solids*, 48 (1987) 635.
24. E. Geidel, F. Billes, *J. Mol. Struc. – Theochem.*, 507 (2000) 75.
25. R.Renjith, J.B. Bhagysree, R.T. Ulahannan, H.T. Varghese, C.Y. Panicker, *Orient. J. Chem.*, 29 (2013) 1.

© 2018 The Authors. Published by ESG (www.electrochemsci.org). This article is an open access article distributed under the terms and conditions of the Creative Commons Attribution license (<http://creativecommons.org/licenses/by/4.0/>).